Identification of intracellular squalene in living algae, *Aurantiochytrium mangrovei* with hyper-spectral coherent anti-Stokes Raman microscopy using a sub-nanosecond supercontinuum laser source

*Kei Ishitsuka[1], Masahiro Koide[2], Masaki Yoshida[2], Hiroki Segawa[3 †], Philippe Leproux[4], Vincent Couderc[4], Makoto M. Watanabe[2], and Hideaki Kano[*1,5,6],*

[1] *Department of Applied Physics, Graduate School of Pure and Applied Sciences, University of Tsukuba, 1-1-1 Tennodai, Tsukuba, Ibaraki, 305-8573, Japan*
[2] *Faculty of Life & Environmental Sciences, University of Tsukuba, 1-1-1 Tennodai, Tsukuba, Ibaraki, 305-8572 Japan*
[3] *Department of Chemistry, School of Science, The University of Tokyo, 7-3-1, Hongo, Bunkyo, Tokyo, 113-0033, Japan*
[4] *Institut de Recherche XLIM, UMR CNRS No. 7252, 123 avenue Albert Thomas, 87060 Limoges CEDEX, France*
[5] *Institute of Applied Physics, University of Tsukuba, 1-1-1 Tennodai, Tsukuba, Ibaraki, 305-8573, Japan*
[6] *Tsukuba Research Center for Interdisciplinary Materials Science (TIMS), University of Tsukuba, 1-1-1 Tennodai, Tsukuba, Ibaraki 305-8571, Japan*

**hkano@bk.tsukuba.ac.jp*

We applied hyper-spectral coherent anti-Stokes Raman scattering (CARS) imaging to intracellular lipid identification in living microalgae, *Aurantiochytrium mangrovei* 18W-13a. Two different lipids, squalene and triacylglycerol (TAG), were found inside living cells with clear vibrational contrast. Based on the endogenous lipid band due to the *cis* C=C stretch vibrational mode, squalene and TAG were clearly distinguished in different intracellular areas. In particular, squalene was detected solely in vacuoles as lipid particles, which was also supported by electron microscopy.

† Present address: National Research Institute of Police Science, 6-3-1, Kashiwanoha, Kashiwa, Chiba 277-0882, Japan

1. Introduction

Algal biomass produced by microalgae has attracted much attention as alternatives of existing energy sources such as fossil fuel and terrestrial plant biomass. Thanks to the biomass production from uncultivated lands and the capability of high lipid storage, microalgae can produce rich amount of lipids more than land plants. So far, a study has been made of high lipid production such as more than 80 % of cell dry mass,[1] which corresponds to several hundred times larger amounts than the biomass which corn can produce[1].

It is well known that triacylglycerols (TAGs) are one of the main lipids microalgae produce. AccumulatedTAGs are, however, not suited for fuels because they consist of oxygen-containing fatty acids. On the other hands, several species such as *Botryococcus braunii* and some *Aurantiochytrium* strains have been reported as they can produce hydrocarbon[2]. Genus *Botryococcus* is classified into *Chlorophyta, Trebouxiophyceae*. Although an autotrophic algae can produce energy through light harvesting, it is not regarded as ideal algae for hydrocarbon production due to its slow growth rate.

Genus *Aurantiochytrium* is a heterotrophic protist, and is classified into *Labyrinthulomycetes*. It mostly inhabits in mangrove forests around subtropical and tropical zones. The unique advantages of *Aurantiochytrium* for biofuel production are its high growth rate and high lipid-accumulation capability. In particular, it maintains the high growth rate in high glucose medium such as 10-12 %[3], and it produces biomass about 70 g/L[4]. *Aurantiochytrium* accumulates saturated fatty acids such as pentadecylic acid and palmitic acid, and polyunsaturated fatty acids such as docosahexaenoic acid (DHA), docosapetaenoic acid (DPA), and eicosapentaenoic acid (EPA). These fatty acids are stored in the form of TAG. In addition to accumulation of TAG, Kaya *et al*. have recently reported accumulation of very high amounts of squalene, which is regarded as one of the most promising next-generation biofuels, by the 18W-13a strain of *A. mangrovei*[5].

Squalene is a polyunsaturated triterpenic hydrocarbon ($C_{30}H_{50}$). It is a key molecule for the biosynthesis of cholesterol, bile acids, and steroids in plants and animals[6]. Squalene is widely used in

cosmetic, medical, and pharmaceutical industries because it serves as a natural antioxidant, inhibitor of chemically induced tumorigenesis, and antifungal agent. Although the major bio-resource of squalene is the liver oil of deep-sea sharks[7], biomass produced by algae has also been used recently[2]. In particular, the 18W-13a strain has been anticipated as an alternative bio-resource for natural squalene.

Making practical use of algae biomass is still challenging. In order to survey the best culture condition for the highest squalene accumulation, current techniques rely on destructive analysis, which are not single-cell analysis. What is more, conventional oleophilic fluorescent dyes, e.g. Nile Red or BODIPY, cannot discriminate squalene from TAG because of their similar hydrophobicities in living cells and tissues. In order to monitor squalene accumulation in real time, and screen special cells with high squalene-accumulation capability, it should be ideal to perform a single-cell analysis in a nondestructive and non-perturbative manner. It can be accomplished by coherent anti-Stokes Raman scattering (CARS) microscopy.

In the CARS process, two laser pulses with different colors are used as ω_1 (pump) and ω_2 (Stokes) pulses. If the angular frequency difference (ω_1 - ω_2) of these two incident laser pulses coincide with the particular angular frequency (Ω) of the vibrational mode of the sample molecule, namely $\omega_1 - \omega_2 = \Omega$, the vibrational mode of a large number of sample molecules is resonantly and coherently excited. The vibrational coherence generated in this process is extracted as ω_{CARS} radiation through the interaction of the molecules with the third laser pulses (ω_3 or probe pulses). According to the energy conservation law, it is required that $\omega_{CARS} = \omega_1 - \omega_2 + \omega_3$ holds. Moreover, based on the phase matching condition (corresponding to the momentum conservation law), the CARS radiation is emitted in the direction of $\mathbf{k}_{CARS} = \mathbf{k}_1 - \mathbf{k}_2 + \mathbf{k}_3$, where $\mathbf{k}_x$ is the wave vector of the ω_x beam. The ω_1 pulses are often used as the ω_3 pulses as well. In such a case, ($\omega_3 = \omega_1$), the signal intensity of the ω_{CARS} radiation is quadratic to the intensity of the ω_1 pulses. In other words, the signal intensity of the ω_{CARS} radiation increases nonlinearly against the intensity of ω_1.

Furthermore, from the phase matching condition, unidirectional radiation can be obtained through the CARS process. After the pioneering works on CARS microscopy[8-10], various kinds of coherent Raman imaging techniques including CARS and stimulated Raman scattering (SRS) have been reported[9-16], and some of them have been summarized in several reviews[13,17,18] or textbooks[19]. In particular, the studies[20-23] and reviews[24,25] on hyper-spectral CARS imaging have also been reported.

Since the CARS process is capable of three-dimensional optical sectioning of a living cell with the sub-cellular spatial resolution, hyper-spectral CARS imaging is expected to differentiate the intracellular lipid molecules. In the present study, we performed label-free molecular imaging using hyper-spectral coherent anti-Stokes Raman scattering (CARS) microscopy, and showed intracellular lipid identification of the 18W-13a strain of *A. mangrovei*.

2. Experimental

2.1. Setup

Figure 1 shows the experimental apparatus for a hyperspectral CARS imaging system we developed[26]. We used a sub-nanosecond microchip laser (repetition rate: 33 kHz, temporal duration: 800 ps, spectral bandwidth: <1 cm^{-1}, average power: about 300 mW, and center wavelength: 1064 nm) as a master laser source. The part of the output was introduced into a photonic crystal fiber (PCF) to generate white-light laser (supercontinuum; SC). Typical input beam power and coupling efficiency of PCF are about 150 mW and 65 %, respectively. The SC had a wide range of spectral components, from visible to near-infrared (NIR), but we used only the NIR components around from 1100 nm to 1700 nm as the broadband Stokes pulses (ω_2). On the other hand, the remaining fundamental from the master laser was used as the pump pulses (ω_1). Both ω_1 and ω_2 pulses were introduced to the microscope in collinear geometry. Two laser pulses are tightly focused on the sample through an objective lens. The CARS radiation generated from the sample was collected using another objective lens, and after passing through

several filters, CARS spectra were measured with a spectrometer and a CCD camera. On the other hand, the other signals due to second or third harmonic generation were also detected using the other spectrometer and the CCD camera. The sample was placed on a three-axis piezo stage, by which we can perform three-dimensional imaging. Typical average powers of the two beams at the sample plane are 10-20 mW for each.

2.2. Sample preparation

Aurantiochytrium mangrovei strain 18W-13a[7] was precultured with 200 mL GTY medium containing 2 % glucose, 1 % tryptone, 0.5 % yeast extract, and 30 % sea water (Coral Pro Salt, Red Sea) in 500 mL Erlenmeyer flasks, which were placed in a temperature-controlled reciprocal shaker (25 °C, 100 strokes min−1,70mm amplitude). After 2 days of preculturing, 1ml of the sample from preculture was inoculated into 200 mL of new GTY medium and cultured for 4 days at the same culture conditions. Cells were sampled in 24, 48, 72, 96 hours later after starting the cultivation. Before measurements, a drop of 50-uL culture medium containing living cells was sandwiched with on a slide glass and cover slip, and it was sealed with manicure.

For electron microscopy, equal volumes of cell suspension and a fixative solution containing 2.5% glutaraldehyde and 0.25M sucrose in 0.05M sodium cacodylate buffer (pH 7.2) were mixed. Fixation was carried out at 4°C for 5 h. After the fixation, cells were pelleted by centrifugation and the pellet was rinsed several times with the same buffer and was fixed with 1% osmium tetroxide for 12 h. The cells were successively dehydrated in 30-100% ethanol series for 10 min each, followed incubation in both ethanol-propylene oxide (PO) mixtures and pure PO twice for 10 min. The dehydrated pellet was embedded in Agar low viscosity resin. The resin was polymerized for 12 h at 70°C. Thin sections were cut on an ultramicrotome and stained for 5 min with 4% uranyl acetate, followed by Sato's lead citrate[27] for 5 min. The sections were viewed with a Hitachi H-7650 TEM.

3. Results and discussion

Figure 2(a) shows an optical image of living algae, which were sampled in 96 hours later after starting the cultivation. The cell size is distributed around from 10 to 30 micrometers in diameter. Figure 2(b) shows a corresponding CARS image of the same cell in Fig. 2(a), which was mapped out just by using the CARS signal intensity at the apparent peak position(2836 cm^{-1}). As well known, the band around 2836 cm^{-1} corresponds to the CH_2 stretch vibrational mode, which is observed mainly in lipids. Since the raw CARS signal is composed of both vibrationally resonant signal and so-called nonresonant background (NRB), those of which interfere with each other (See Fig. 2(c)). In order to extract pure vibrationally resonant signal, we performed numerical analysis called maximum entropy method (MEM)[28]. The spectral profile of the pure vibrationally resonant signal, which corresponds to imaginary part of $\chi^{(3)}$(Im[$\chi^{(3)}$]), is shown in Fig. 2(d). The spectral profile in Fig. 2(d) agrees well with that of intracellular TAG in algae[29,30]. One of the unique characteristics in Fig. 2(d) is abundance of unsaturated lipids. This is manifested by the intense band at 2996 cm^{-1}, which corresponds to the C-H stretch mode of C=C-H bonds.

By analyzing the spectral profile at each cell position, we reconstructed CARS images at various Raman bands. Figure 3 summarizes the results of hyper-spectral CARS imaging. Figures 3(b-i) show CARS images at 2996(b), 2914(c), 2840(d), 1738(e), 1439(f), 1379(g), 1324(h), and 1265(i) cm^{-1}. As clearly shown, microscopic intracellular structures are visualized. In particular, particle-like structures with diameter of a few micrometers are observed in Figs.3(b), (d), (e), (f), and (i). These bands are assigned as the C-H stretch mode of C=C-H bonds(b), CH_2 stretch vibrational mode(d), C=O stretch mode of ester(e), CH bend mode(f), and CH bend mode of C=C-H bonds(i). The spectral profile at a particle-like structure, indicated as A in Fig. 3(d) (the same as shown in Fig. 2(b)), is depicted in Fig. 4(a). It should be also

noticed that CH_2 stretch vibrational mode in Fig. 3(d) shows intense signal in the other area indicated as B. The same trends are also found in Figs. 3(g) and (h).

Based on the optical image in Fig. 3(a), the area around B seems to correspond to a vacuole, at which the band at 2914 cm^{-1} (CH_3 stretch vibrational mode) due to lipids and proteins is also weakly found. The spectral profile indicated as B in Fig. 3(d) is shown in Fig. 4(b). Although both spectra give intense signal at the CH_2 stretch vibrational mode, the spectral profiles are completely different. It suggests that at least two kinds of lipids should be accumulated in cells.

In order to identify molecular species which give the spectra in Figs. 4(a) and (b), we carried out the measurement of standard samples of two kinds of lipids, which are known as intracellular lipids in *Aurantiochytrium* using the same experimental setup. Figures 4(c) and (d) show spectral profiles of triolein, which is one of the TAG families found in algae, and squalene. Both of triolein and squalene are purchased (WAKO Japan) and used without further purification. The spectral profiles of (a) and (c) ((b) and (d)) coincide well with each other. In particular, both bands at 1379 and 1324cm^{-1} in Figs. 3(g) and (h) are assigned as CH_3 deformation modes of squalene[31], which are also observed in Fig. 4(b) and (d). Therefore, the lipids at the positions of A and B are assigned as TAG and squalene, respectively.

Among the vibrational marker bands of squalene and TAG, the band around 1650 cm^{-1} is prominent and is assigned as *cis* C=C stretch vibrational mode. Figure 5 shows close-up spectral profile of the band around 1650 cm^{-1} in Fig. 4(a) and (b). It is clear that the peak position of the bands due to *cis* C=C stretch vibrational mode are different between squalene (green) and TAG (blue). Moreover, it should also be noted that the spectral profile due to TAG also shows the band at 1738 cm^{-1}. This band is assigned as the C=O stretch vibrational mode of the ester bonds, which should be absent from the spectrum of squalene. The peak positions of the bands due to *cis* C=C stretch vibrational mode of TAG and squalene in Figs. 4(a) and (b) are determined to be 1654 and 1665 cm^{-1}, respectively, by fitting the bands using a Gaussian

function. These coincide well with the peak positions at 1652 and 1666 cm^{-1} for neat TAG and squalene in Figs. 4(c) and (d), respectively. Although the bands at 1379 and 1324 cm^{-1} can also be used as marker bands of squalene, the amplitude of the band around 1650 cm^{-1} was more than 5 times larger than that at 1379 and 1324 cm^{-1}.In what follows, we thus used the band around 1650 cm^{-1} for the quantitative analysis of squalene.

In order to differentiate intracellular squalene and TAG in the field of view shown in Fig. 3, we fitted the bands around 1650 cm^{-1} using the sum of two Gaussian functions, whose peak positions are fixed to be 1665 and 1654 cm^{-1}. Figures 6(a), (b), and (c) show the optical image of the cells (a) and the fitted results of the images for squalene (b) and TAG (c). These images ((b) and (c)) show that squalene and TAG do not co-localize with each other in spite of their common hydrophobic profiles in protoplasm. It should be noted that the areas where squalene is found correspond to round pore-like organelles, which considered to be vacuoles. Figure 7 shows the close-up image of the optical image(a), that of squalene (b), and an image obtained by electron microscopy (c). Note that the cells in Figs. 7(a-b) and 7(c) are different. Several small round particles are found in vacuole in Figs. 7(a) and (b), those of which should correspond to the spots indicated as arrows(green) in Fig. 7(c). The possible reasons of squalene storing in vacuole is temporary storage of excess amount, recycling as energy or carbon source by decomposition. Since squalene is stored as a small lipid particle in vacuoles, the particles are trapped and dragged by the incident laser pulses due to laser tweezing effect. This is manifested by the horizontal stripes in vacuoles in Fig. 7(b). Since the CARS image is acquired by translating the sample stage with raster scanning, the horizontal stripes are caused by the laser tweezing effect of squalene particle.

As clearly shown, hyper-spectral CARS microscopy is capable of differentiating between squalene and TAG in living algae, which has been difficult with the use of other techniques such as

fluorescence imaging and electron microscopy. Since this method can trace a living cell *in situ* and *in vivo*, it is useful to optimize the cultural condition for the best capability of squalene production.

Next, we performed incubation-time-dependent hyper-spectral CARS imaging. Cells were sampled in 24, 48, 72, 96 hours later after starting the cultivation. Figure 8 shows the results of an optical image(a), CARS at *cis* C=C stretch vibrational mode of squalene(b), CARS at *cis* C=C stretch vibrational mode of TAG(c), and second harmonic generation (SHG)(d). As clearly shown in Figs. 8(b) and (c), both of lipids, squalene and TAG, were accumulated in 72 and 96 hours. In particular, squalene was profoundly observed in 96 hours. It should be noted that squalene particles in vacuoles are dragged through the laser tweezing effect. Since this effect is prominent for large vacuoles, the signal intensity does not directly correspond to the local existence of squalene molecules.

In the present study, we unexpectedly found SHG spots only in 24 hours. In general, SHG takes place if there is highly polarizable and well-ordered non-centrosymmetric molecular organizations or structures with SHG-active molecules[32,33]. Therefore, such a structure should exist in the SHG-active areas. As biophysical probes for rounding up specific molecular structures, mitotic spindles[34], contractile filaments in muscle[34], muscle myosin[35], axons[36] have been reported so far. Since SHG was observed only in 24 hours, it should be related to the cell cycle of *A. mangrovei*. It is reported that *A. limacinum*, another species of the genus *Aurantiochytrium*, give rise to zoospores regularly in 24 h after the inoculation to a new media[37]. Zoospore formation of *Aurantiochytrium* is thus time-specific development around 24 hours of cultivation, at which the sequential mitosis takes place within a single cell prior to cytokinesis[38]. In addition, active restructuring of cytoskeletons will occur to compose heterokont flagella and flagellar apparatus at the same moment. After 24 hours, it shows a normal mitosis process of spherical vegetative cells without flagella. Since the formation of zoospore is one of the important checkpoints for cell growth and subsequent squalene accumulation, it is highly desirable to visualize this timing for a living cell with a

label-free method. We are now identifying the SHG-active molecular origin, and will be reported in the forthcoming paper.

4. Conclusion

With the use of hyperspectral CARS imaging, we succeeded in visualizing molecular species in living algae, *Aurantiochytrium mangrovei*. In particular, the vibrational band assigned as the *cis* C=C stretch vibrational mode was found to be useful to distinguish intra-cellular lipids such as squalene and TAG. Since this technique is label-free, non-destructive, non-contact, and low-invasive, the real-time accumulation process of squalene could be monitored at the sub-cellular level. Using the label-free Raman marker band of the *cis* C=C stretch vibrational mode, we can sort the cells with high productivity of squalene. Moreover, another label-free technique, SHG provided unique organelle specificity. Since the observation of SHG took place only at 24 hours, the SHG-active organelle should be related to sequential mitosis process.

Acknowledgement

This study was financially supported by Photographic Research Fund of Konica Minolta Imaging Science Foundation to HK, and JSPS KAKENHI Grant Number 23770234 and Mayekawa Houonkai Foundation to MY. The authors thank the LEUKOS company for technical support with the dual-output supercontinuum light source. The authors gratefully acknowledge J. Ukon, UKON CRAFT SCIENCE, Ltd. for assisting with a fruitful collaboration between Japanese and French labs.

References

(1) Chisti Y *Biotechnol. Adv.* **2007**, *25*, 294.

(2) Yoshida M, Tanabe Y, Yonezawa N, Watanabe MM *Biofuels* **2012**, *3*, 761.

(3) Nakazawa A, Matsuura H, Kose R, Ito K, Ueda M, Honda D, Inouye I, Kaya K, Watanabe MM *Procedia Environ. Sci.* **2012**, *15*, 27.

(4) Lee Chang KJ, Dumsday G, Nichols PD, Dunstan GA, Blackburn SI, Koutoulis A *Appl. Microbiol. Biotechnol.* **2013**, *97*, 6907.

(5) Kaya K, Nakazawa A, Matsuura H, Honda D, Inouye I, Watanabe MM *Biosci. Biotechnol. Biochem.* **2011**, *75*, 2246.

(6) Smith TJ *Expert Opin. Inv. Drug* **2000**, *9*, 1841.

(7) Hernandez-Perez M, Gallego RMR, Alayon PJP, Hernandez AB *Mar. Freshwater Res.* **1997**, *48*, 573.

(8) Duncan MD, Reintjes J, Manuccia TJ *Opt. Lett.* **1982**, *7*, 350.

(9) Zumbusch A, Holtom GR, Xie XS *Phys. Rev. Lett.* **1999**, *82*, 4142.

(10) Hashimoto M, Araki T, Kawata S *Opt. Lett.* **2000**, *25*, 1768.

(11) Cheng J-X, Xie XS *J. Phys. Chem. B* **2004**, *108*, 827.

(12) Volkmer A *J. Phys.D: Appl. Phys.* **2005**, *38*, R59.

(13) Evans CL, Xie XS *Annu. Rev. Anal. Chem.* **2008**, *1*, 883.

(14) Day JPR, Domke KF, Rago G, Kano H, Hamaguchi H, Vartiainen EM, Bonn M *J. Phys. Chem. B* **2011**, *115*, 7713.

(15) Freudiger CW, Min W, Saar BG, Lu S, Holtom GR, He C, Tsai JC, Kang JX, Xie XS *Science* **2008**, *322*, 1857.

(16) Saar BG, Freudiger CW, Reichman J, Stanley CM, Holtom GR, Xie XS *Science* **2010**, *330*, 1368.

(17) Cheng JX, Xie XS *J. Phys. Chem. B* **2004**, *108*, 827.

(18) Day JPR, Domke KF, Rago G, Kano H, Hamaguchi H, Vartiainen EM, Bonn M *J. Phys. Chem. B* **2011**, *115*, 7713.

(19) Dudovich N, Oron D, Silberberg Y *Nature* **2002**, *418*, 512.

(20) Kee TW, Zhao HX, Cicerone MT *Opt. Express* **2006**, *14*, 3631.

(21) Kano H, Hamaguchi H *Appl. Phys. Lett.* **2005**, *86*.

(22) Petrov GI, Yakovlev VV *Opt. Express* **2005**, *13*, 1299.

(23) Camp CH, Jr., Lee YJ, Heddleston JM, Hartshorn CM, Hight Walker AR, Rich JN, Lathia JD, Cicerone MT *Nat. Photonics* **2014**, *8*, 627.

(24) Kano H, Segawa H, Leproux P, Couderc V *Opt. Rev.* **2014**, *21*, 752.

(25) Kano H, Segawa H, Okuno M, Leproux P, Couderc V *J. Raman. Spectrosc.* **2016**, *47*, 116.

(26) Okuno M, Kano H, Leproux P, Couderc V, Day JPR, Bonn M, Hamaguchi H *Angew. Chem. Int. Ed.* **2010**, *49*, 6773.

(27) Sato T *J. Electron Microsc. (Tokyo)* **1968**, *17*, 158.

(28) Vartiainen EM, Rinia HA, Müller M, Bonn M *Opt. Express* **2006**, *14*, 3622.

(29) Wu HW, Volponi JV, Oliver AE, Parikh AN, Simmons BA, Singh S *P. Natl. Acad. Sci. USA.* **2011**, *108*, 3809.

(30) Fu D, Lu FK, Zhang X, Freudiger C, Pernik DR, Holtom G, Xie XS *J. Am. Chem. Soc.* **2012**, *134*, 3623.

(31) Chun HJ, Weiss TL, Devarenne TP, Laane J *J. Mol. Struct.* **2013**, *1032*, 203.

(32) Huang JY, Lewis A, Loew L *Biophys. J.* **1988**, *53*, 665.

(33) Rasing T, Huang J, Lewis A, Stehlin T, Shen YR *Phys. Rev. A* **1989**, *40*, 1684.

(34) Campagnola PJ, Millard AC, Terasaki M, Hoppe PE, Malone CJ, Mohler WA *Biophys. J.* **2002**, *82*, 493.

(35) Plotnikov SV, Millard AC, Campagnola PJ, Mohler WA *Biophys. J.* **2006**, *90*, 693.

(36) Dombeck DA, Kasischke KA, Vishwasrao HD, Ingelsson M, Hyman BT, Webb WW *Proc. Natl. Acad. Sci. U.S.A.* **2003**, *100*, 7081.

(37) Morita E, Kumon Y, Nakahara T, Kagiwada S, Noguchi T *Mar. Biotechnol.* **2006**, *8*, 319.

(38) Honda D, Yokochi T, Nakahara T, Erata M, Higashihara T *Mycol. Res.* **1998**, *102*, 439.

Figure 1. Experimental setup of hyper-spectral CARS microspectroscopic system[47].

Figure 2. Optical image of living algae *A. mangrovei* strain 18W-13a, which were sampled in 96 hours later after starting the cultivation(a). The bright spot at the center corresponds to the laser spot; CARS image at 2836 cm^{-1}(b); Raw CARS spectrum at the position indicated as a green cross in (b) (c); Im[$\chi^{(3)}$] spectrum calculated from (c) (d).

Figure 3. Optical image of *A. mangrovei* strain 18W-13a (the same image as Fig. 2(a)) (a); CARS images at 2996(b), 2914(c), 2840(d), 1738(e), 1439(f), 1379(g), 1324(h), and 1265(i) cm^{-1}. The spectral profiles at two positions indicated as A and B in (d) are shown in Fig. 4.

Figure 4. Spectral profiles((a) and (b)) at two intracellular positions indicated as A and B in Fig. 3(d), respectively; Spectral profiles((c) and (d)) of neat triolein and squalene, which are main two intracellular lipids in *Aurantiochytrium*.

Figure 5. Close-up spectral profiles of the band around 1654 cm^{-1} for squalene (green) and TAG (blue), which are shown in Fig. 4(a) and (b). The band at 1738 cm^{-1} in blue curve corresponds to the C=O stretch vibrational mode of the ester bonds.

Figure 6. Optical image (the same image as Fig. 2(a)) (a) and fitted results of squalene (b) and TAG (c).

Figure 7. Close-up image of the optical image shown in Fig. 6(a) (a), CARS image due to squalene (Fig. 6(b)) (b), and an image obtained by electron microscopy(c). Green arrows indicate lipid particles in a vacuole.

Figure 8. Incubation-time-dependent hyper-spectral CARS imaging. Cells were sampled in 24, 48, 72, 96 hours later after starting the cultivation. optical image(a), CARS at *cis* C=C stretch vibrational mode of squalene(b), CARS at *cis* C=C stretch vibrational mode of TAG(c), and second harmonic generation (SHG)(d).

Graphical Abstract

Identification of intracellular squalene in living algae, *Aurantiochytrium mangrovei* with hyper-spectral coherent anti-Stokes Raman microscopy using a sub-nanosecond supercontinuum laser source

Kei Ishitsuka, Masahiro Koide, Masaki Yoshida, Hiroki Segawa, Philippe Leproux, Vincent Couderc, Makoto M. Watanabe, and Hideaki Kano

Incubation-time-dependent hyper-spectral CARS imaging. Cells were sampled in 24, 48, 72, 96 hours later after starting the cultivation. optical image(a), CARS at *cis* C=C stretch vibrational mode of squalene(b), CARS at *cis* C=C stretch vibrational mode of TAG(c), and second harmonic generation (SHG)(d).

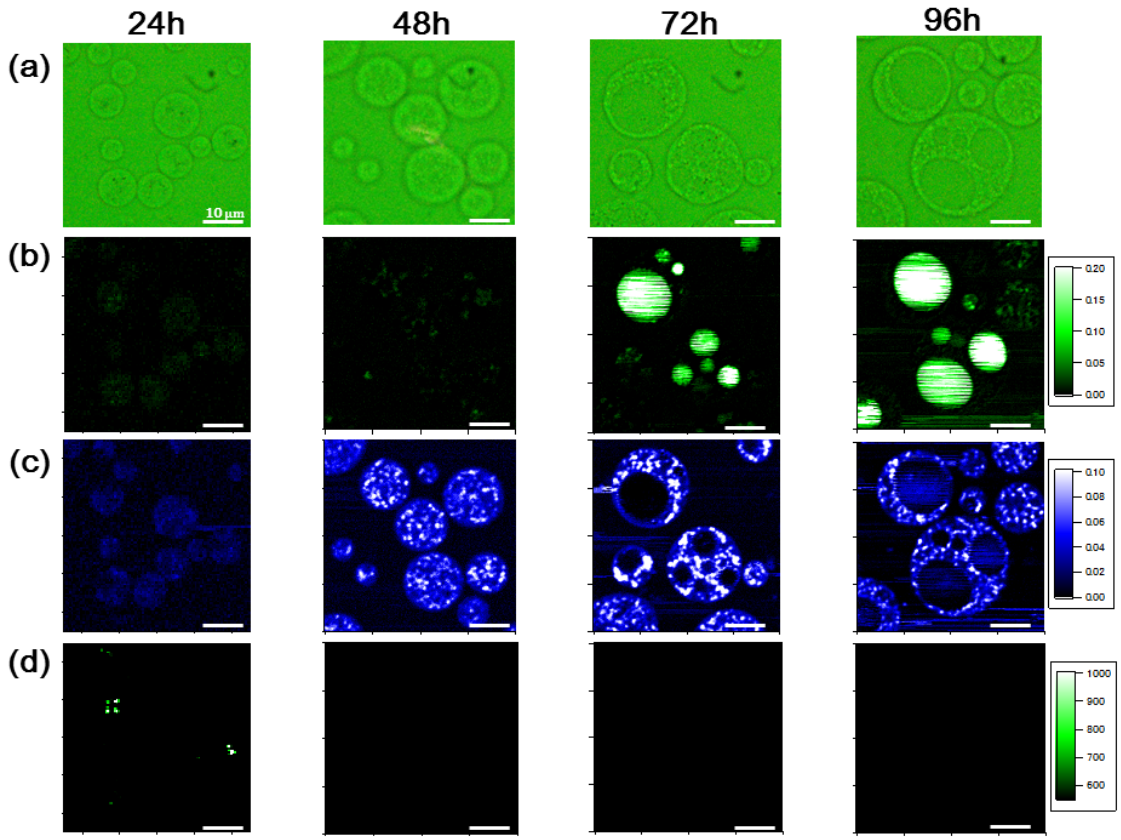

Fig. 1

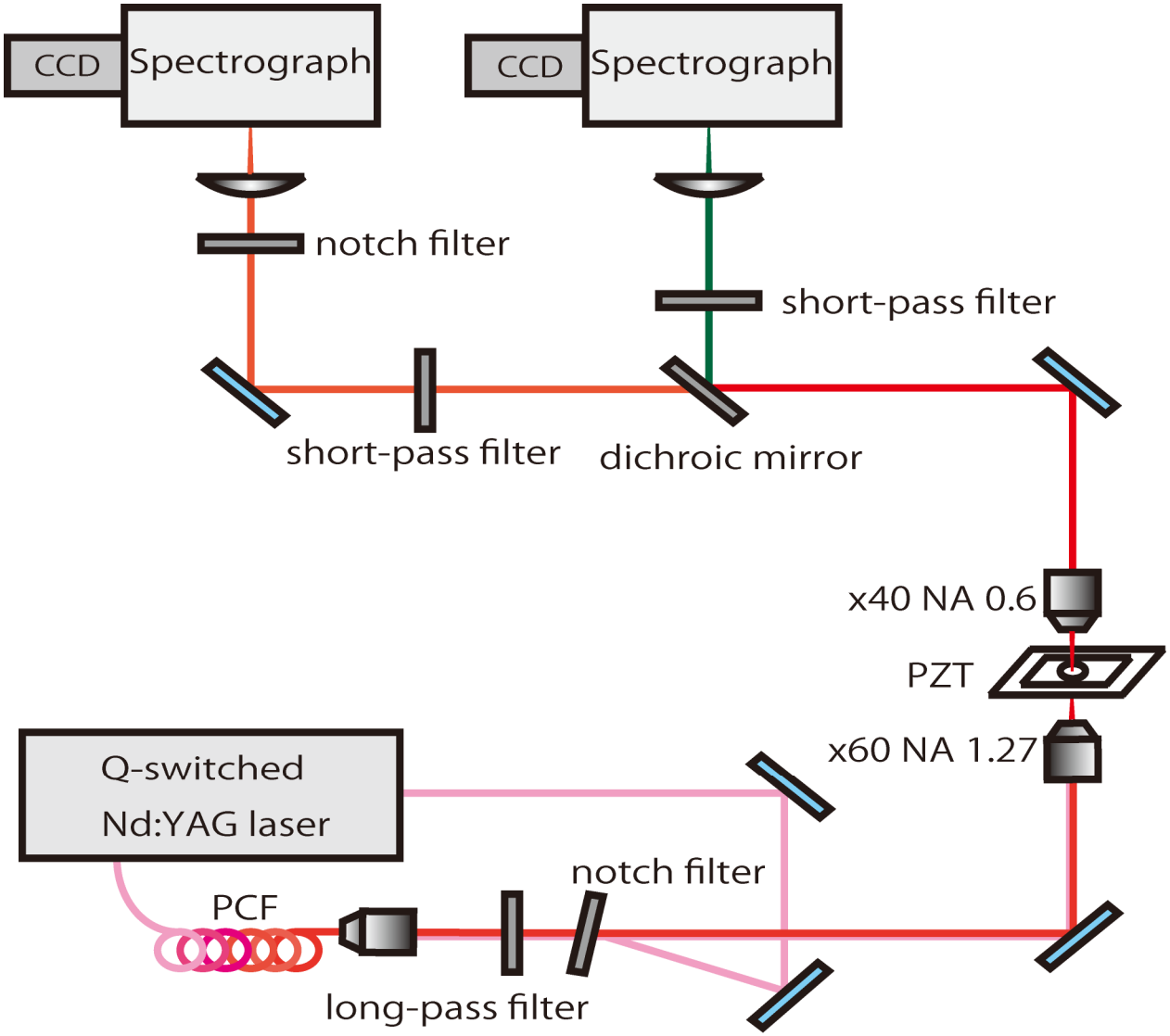
CCD
Spectrograph
CCD
Spectrograph
notch filter
short-pass filter
short-pass filter
dichroic mirror
x40 NA 0.6
PZT
x60 NA 1.27
Q-switched
Nd:YAG laser
notch filter
PCF
long-pass filter

Fig. 2

(a)

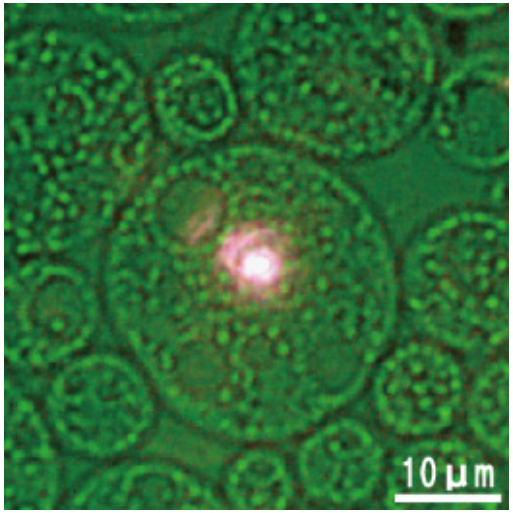
10 µm

(b)

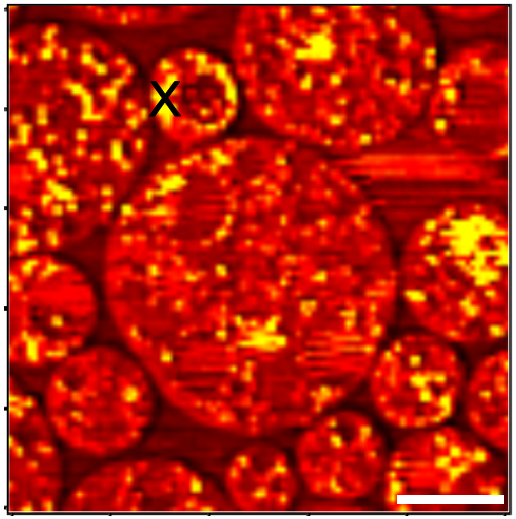
X

(c)

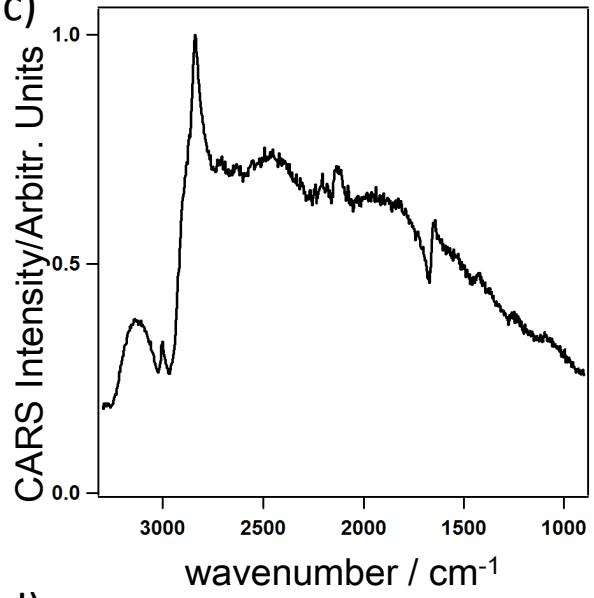
CARS Intensity/Arbitr. Units
1.0
0.5
0.0
3000
2500
2000
1500
1000
wavenumber / cm-1

(d)

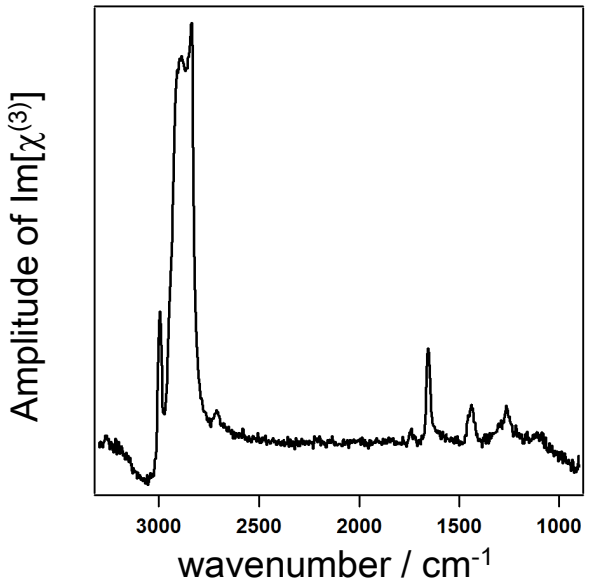
Amplitude of Im[χ(3)]
3000
2500
2000
1500
1000
wavenumber / cm-1

Fig. 3

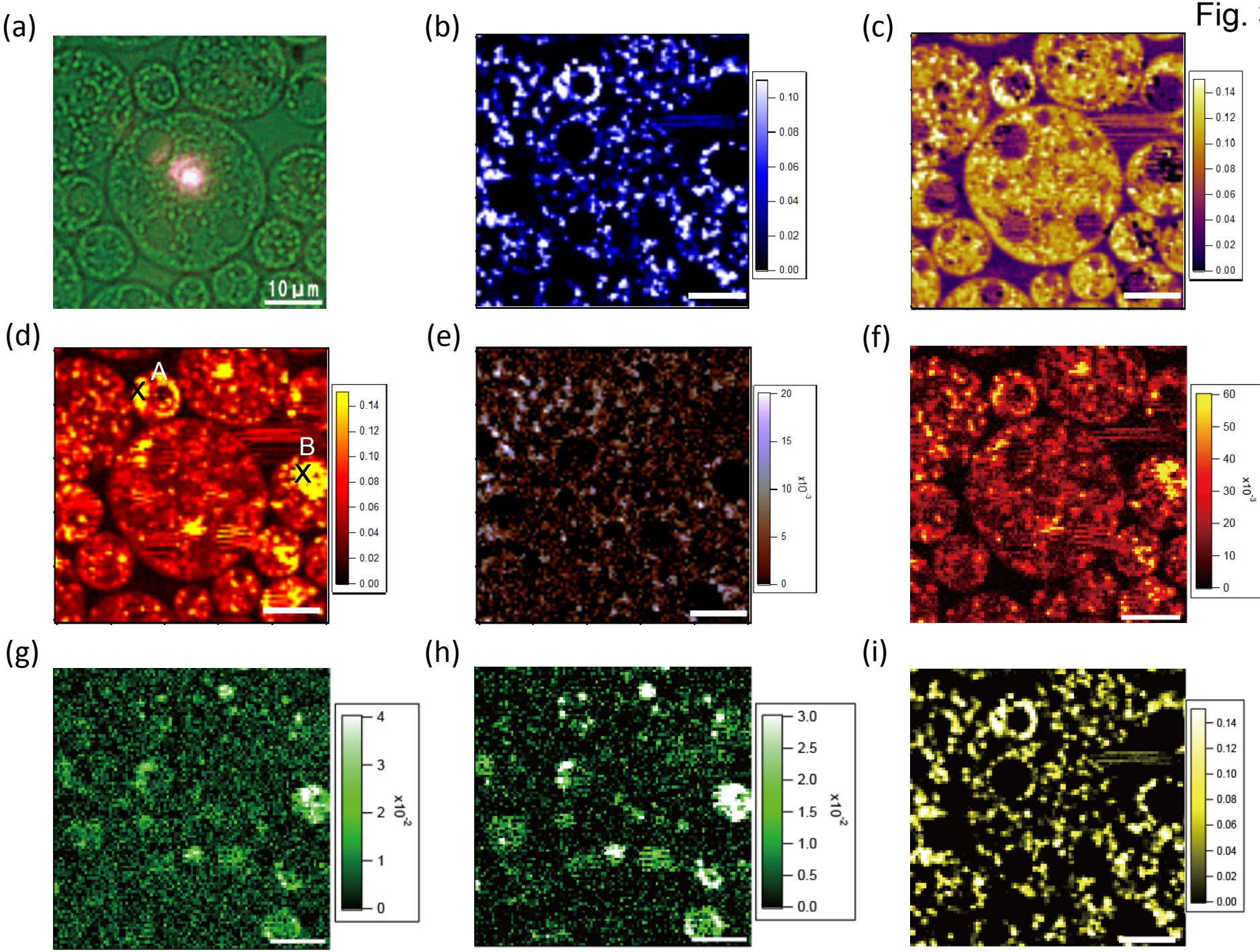
(a)
10 µm
(b)
0.10
0.08
0.06
0.04
0.02
0.00
(c)
0.14
0.12
0.10
0.08
0.06
0.04
0.02
0.00
(d)
A
B
0.14
0.12
0.10
0.08
0.06
0.04
0.02
0.00
(e)
20
15
10
5
0
x10-3
(f)
60
50
40
30
20
10
0
x10-3
(g)
4
3
2
1
0
x10-2
(h)
3.0
2.5
2.0
1.5
1.0
0.5
0.0
x10-2
(i)
0.14
0.12
0.10
0.08
0.06
0.04
0.02
0.00

Fig 4

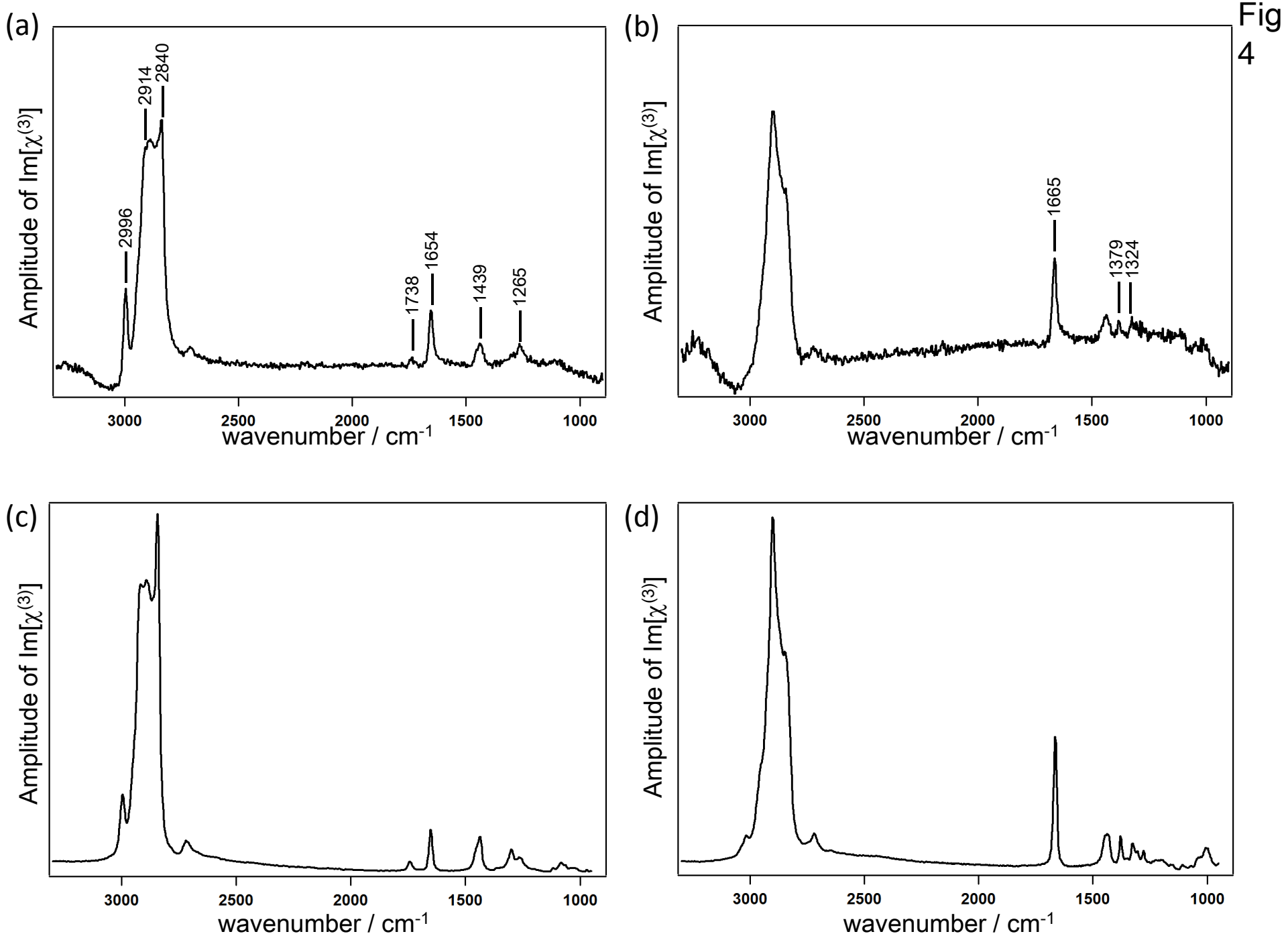
(a)
Amplitude of Im[χ(3)]
2914
2840
2996
1738
1654
1439
1265
3000
2500
2000
1500
1000
wavenumber / cm-1
(b)
Amplitude of Im[χ(3)]
1665
1379
1324
3000
2500
2000
1500
1000
wavenumber / cm-1
(c)
Amplitude of Im[χ(3)]
3000
2500
2000
1500
1000
wavenumber / cm-1
(d)
Amplitude of Im[χ(3)]
3000
2500
2000
1500
1000
wavenumber / cm-1

Fig. 5

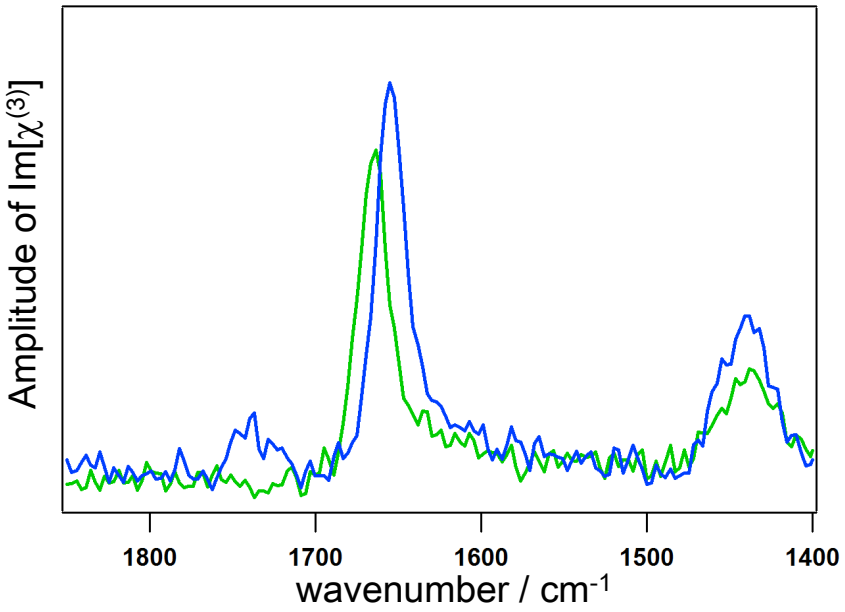
Amplitude of Im[$\chi^{(3)}$]
1800
1700
1600
1500
1400
wavenumber / cm^{-1}

Fig. 6

(a)

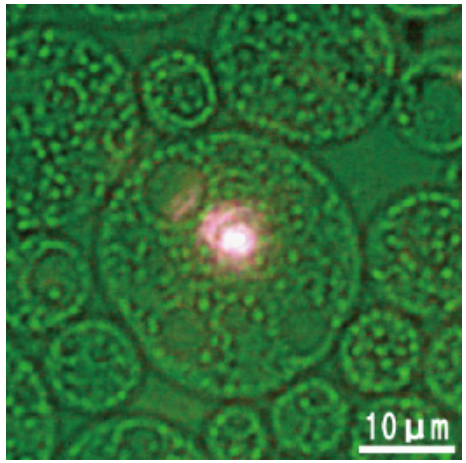

(b)

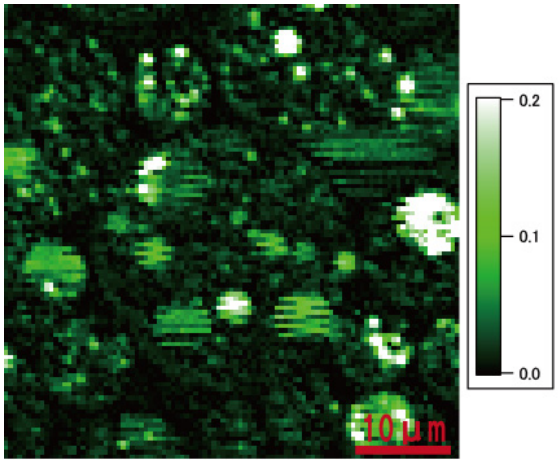

(c)

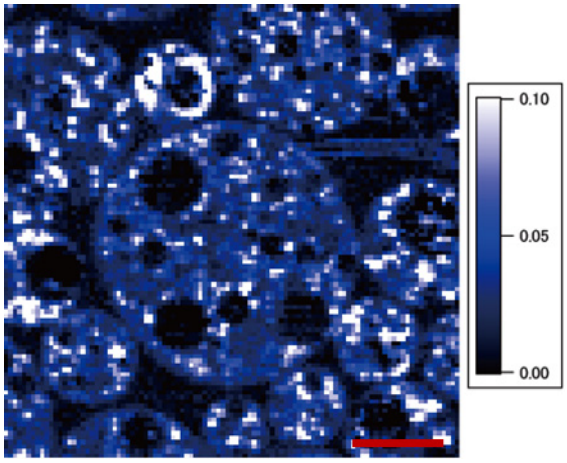

Fig. 7

(a)

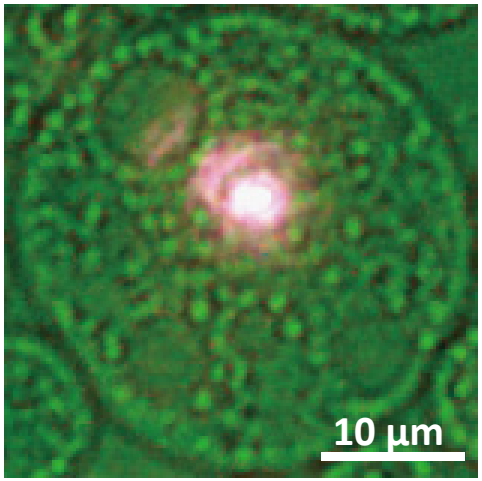

(b)

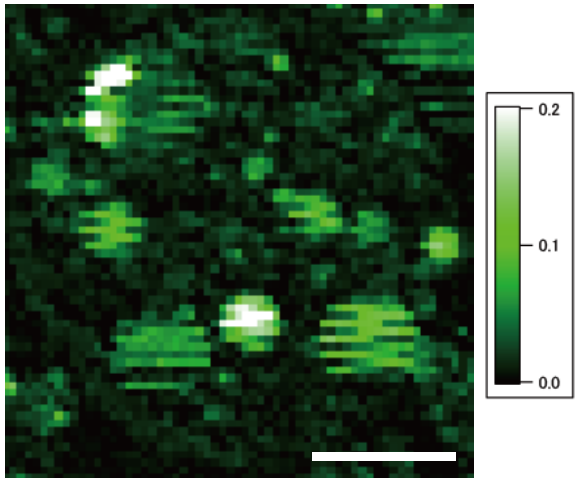

(c)

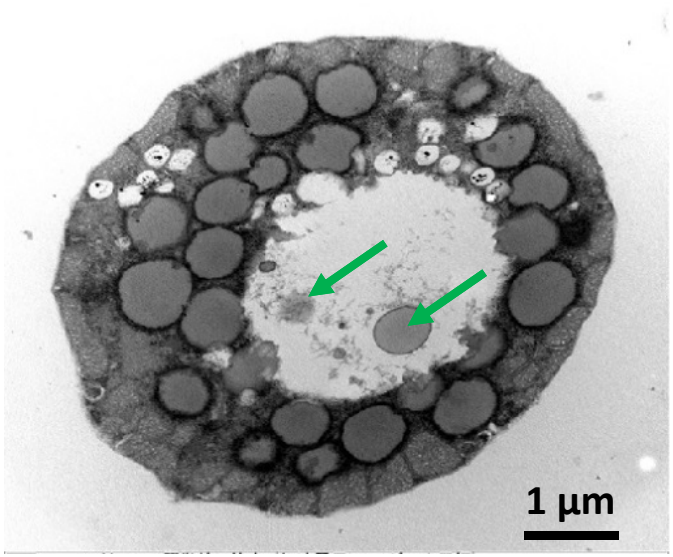

Fig. 8

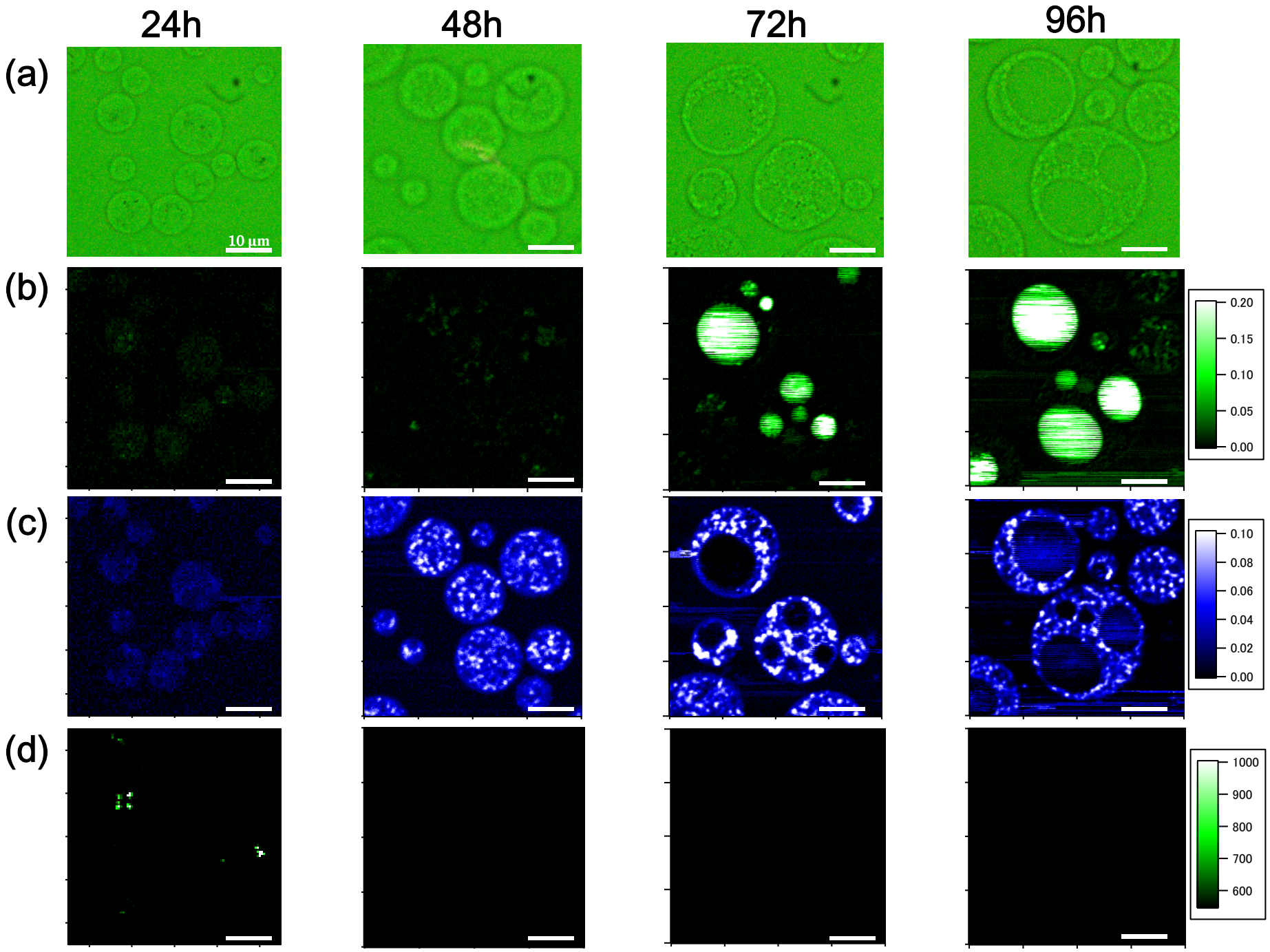
24h
48h
72h
96h
(a)
(b)
(c)
(d)
10 μm
0.20
0.15
0.10
0.05
0.00
0.10
0.08
0.06
0.04
0.02
0.00
1000
900
800
700
600